

Contribution to the textural characterisation of Filtrasorb 400 and other commercial activated carbons commonly used for water treatment

Catherine Morlay · Jean-Pierre Joly

Published online: 14 August 2009
© Springer Science+Business Media, LLC 2009

Abstract The textural characteristics of three commercial activated carbons, Filtrasorb 400 (F400), Industrial React High Affinity and Picabiol, commonly used in water treatment, are reinvestigated. Nitrogen physisorption isotherms are determined in the range $P/P_0 = [4 \times 10^{-7}$ –0.998] and processed using BET, α_S (Sing), Dubinin–Radushkevich and Density Functional Theory methods. In addition, fractal dimensions are determined by the Frenkel–Halsey–Hill procedure. Since F400 is often considered as a reference material in studies on the adsorption of solutes in aqueous solutions, a review of the textural characteristics of this carbon is carried out. The results obtained in this work using the different methods are consistent and a critical crossed comparison of these results allows discussing the limitations of the methods used. In particular, the impact of the P/P_0 range considered on S_{BET} value is examined. In addition, the accuracy of the BET specific surface area is assessed in the light of information from recent literature.

Keywords Filtrasorb 400 · Activated carbon · Mercury porosimetry · BET · Alpha-S · DR · DFT

C. Morlay (✉) · J.-P. Joly
Université Lyon 1, CNRS, UMR 5256, IRCELYON (Institut de Recherches sur la Catalyse et l’Environnement de Lyon), Université de Lyon, 69622 Villeurbanne, France
e-mail: catherine.morlay@ircelyon.univ-lyon1.fr

C. Morlay
NanoScience Technology Center, University of Central Florida, 12424 Research Parkway, Orlando, FL 32826, USA

1 Introduction

The understanding of thermodynamics and kinetics of adsorption from liquid solutions needs, among other requirements, a detailed characterisation of the porous system of the adsorbent [1, 2]. Activated carbons (ACs) are generally well-suited for water purification because of a good arrangement of their mesoporous and microporous systems. In addition, the specific surface area of the pore walls found in activated carbons is a factor of major importance in discussing adsorption at molecular level [3–6].

The ACs considered in this work are Filtrasorb 400 (F400), Industrial React High Affinity (IRHA) and Picabiol (PBL). F400 and PBL are both used for drinking water treatment but for different purposes. F400 is specially recommended to remove organic micropollutants such as pesticides. PBL is used when, besides the “pure” adsorption phenomenon, a bacterial growth on the AC surface is to be favoured. On the other hand, IRHA is specially recommended for industrial wastewaters discoloration. Finally, F400 is often quoted in the literature in studies dealing with adsorption in aqueous medium and consequently it is an interesting material for data comparison purposes.

The aim of this work was to focus on the critical assessment of the textural characteristics of these commercial ACs in the light of a review of the results available for F400 in literature.

2 Materials

F400, IRHA and PBL are commercialized as granular ACs. F400 and IRHA are Chemviron Carbon (European

Table 1 General information relative to the activated carbons considered

Activated carbon	Manufacturer	Raw material	Activation process	Surface area ^a (m ² g ⁻¹)	Average particle size after grinding ^a (μm)
Filtrasorb 400 (F400)	Chemviron Carbon	Bituminous coal	Physical (steam)	1,050	40
Industrial React High Affinity (IRHA)	Chemviron Carbon	Bituminous coal	Physical (steam)	950	40
Picabiol (PBL)	Pica	Pine wood	Chemical (H ₃ PO ₄)	1,500	25

^a Values given by the manufacturer

Operations of Calgon Carbon Corporation, USA) products and PBL is a Pica (France) product. Table 1 gathers some general information which was provided by the producers of these ACs including the average size of the particles after grinding. F400 and IRHA are physically activated (steam) whereas wood based PBL is chemically activated (H₃PO₄). The three ACs were used as received. For any determination, the powdered ACs were dried in an oven (130 °C, at least for 24 hours) before weighting.

3 F400 textural results from literature

As F400 is often used in studies dealing with adsorption from aqueous solution, numerous data have been published on its textural characteristics. Table 2 gathers some of these data which we selected as enough details were provided by the authors relative to the operative conditions in which they were obtained [7–17]. In addition, an international inter-laboratory trial for the determination of activated carbon pore volume distributions of four activated carbons (including F400 and a wood-based, chemically activated carbon similar in properties to Picabiol) has been performed [18].

Table 2 does not evidence any significant influence of a prior water washing and subsequent drying on F400

textural characteristics. The values reported for V_p , volume including micropores and mesopores, are dispersed in the range 0.49–0.70 cm³ g⁻¹ and S_{BET} values are dispersed in the range 816–1,174 m² g⁻¹. The mean values of S_{BET} and V_p are 1,005 m² g⁻¹ and 0.58 cm³ g⁻¹, respectively, with corresponding standard deviations of 97 m² g⁻¹ and 0.06 cm³ g⁻¹. The mean microporous volume is equal to 0.4 cm³ g⁻¹ and the standard deviation is 0.07. Data dispersion can originate from differences in the operative conditions chosen to carry out the nitrogen physisorption experiments. In particular, S_{BET} values might depend on the relative pressure range chosen for its determination.

In order to amplify and discuss these results from the literature, we carried out our own investigations on the textural characteristics of F400. Carbons IRHA and PBL were also studied for comparison purposes. The experimental conditions used are described below.

4 Methods and textural characterization

Mercury porosimetry experiments were carried out using a Micromeritics instrument (AutoPore IV 9500 model) within the pressure range 3×10^{-3} –413.5 MPa. Prior to the experiments, each sample was dried at 130 °C under air for 60 h. Applied pressures and subsequent intruded

Table 2 F400 textural characteristics found in literature

S_{BET} (m ² g ⁻¹)	P/P_0 domain for S_{BET}	Previous outgassing	V_p (cm ³ g ⁻¹); P/P_0	V_{micro} (cm ³ g ⁻¹); method	S_{micro} (m ² g ⁻¹); method	Reference
1,174	0.05–0.35	120 °C; 1.5 h	0.6; 0.9814	0.32; t-plot	718; t-plot	Tsang et al. [7]
1,035	0.01–0.1	–	0.55; 0.98	0.4; DR	–	Dastgheib et al. [11]
993 (washed)	0.03–0.111	–	0.615; 0.992	0.373; t-plot	893; t-plot	Lu and Sorial [13]
866.4	–	–	0.567; 0.98	0.301; t-plot	635.9; t-plot	Alvarez et al. [9]
1,009	0.01–0.03	200 °C; 2 h	0.54; 0.95	0.38; DR	–	Yue et al. [17]
1026.5 (washed)	–	–	–	0.423; –	–	Canizares et al. [10]
1,020	–	70 °C; 10 ⁻⁵ Torr	0.70; 0.95	0.50; DR	–	Al-Degs et al. [8]
1,000	–	–	–	0.474; α_S	946; α_S	Rivera-Utrilla and Sanchez-Polo [15]
1,018 (washed)	0.01–01	110 °C; 16 h	0.54; 0.95	0.47; $P/P_0 = 0.4$	–	Newcombe and Drikas [14]
816	–	110 °C; 16 h	0.489; –	–	–	Skradas et al. [16]
1,100	–	50 °C 0.1 Pa; 18 h	–	–	1045; t-plot	Garnier et al. [12]

volumes of mercury data were computed assuming a slit-shaped geometry of the pores. The PSD of each AC was thus obtained within the pore width range 2.1 nm–300 µm. The relation between the applied pressure and the width of the pores into which mercury intrudes is given by the Laplace equation [19] for a cylindrical meniscus occurring in a slit-shaped pore:

$$W = -2\gamma \cos(\theta)/P \quad (1)$$

where P , W , γ and θ denote the mercury penetration equilibrated pressure, the width of the pore being intruded, the surface tension of mercury (485×10^{-3} N m⁻¹ at 25 °C) and the contact angle between mercury and the pore wall (155° with carbon according to ASTM standard D4284-92), respectively. A slit-shaped model has been chosen to describe meso and macropores for a question of homogeneity of analysis with the conventional DFT (NLDFT) method. However, if this model is commonly admitted for micropores, its application to wider pores, and especially to macropores, is not obvious [20]. Consequently, the comparison between the PSDs given by both methods in their overlapping pore size range is qualitative.

Nitrogen adsorption–desorption isotherms were determined at 77.4 K for equilibrium relative pressures, P/P_0 , in the range 4×10^{-7} –0.995 using a Micromeritics instrument (ASAP 2010 V5.02 model). Prior to the experiments, each sample was outgassed at 120 °C under high vacuum. Nitrogen adsorption–desorption data were processed using Brunauer, Emmet and Teller (BET) [21], Dubinin–Radushkevich (DR) [22], α_S (Sing) [23] and Density Functional Theory (DFT) [24] methods and Frenkel–Halsey–Hill (FHH) procedure. In the following, macro-, meso- and micro-pores refer to the definitions given by IUPAC [25].

BET specific surface areas S_{BET} were calculated within the relative pressure range $P/P_0 = 0.01$ –0.1. The porous volume including meso- and micropores, V_p , was calculated from the amount of nitrogen adsorbed at $P/P_0 = 0.995$, considering the density of liquid nitrogen at 77.4 K being equal to 0.8081 g cm⁻³.

The DR method was applied in the isotherm region $P/P_0 = 10^{-4}$ – 10^{-2} [22, 26]. Physisorption in a micro-porous material is modelled by the following equation:

$$V = V_{\text{micro}} \exp\left\{-[A/(\beta E_0)]^2\right\} \quad (2)$$

with:

$$A = RT \ln(P_0/P) \quad (3)$$

where V , V_{micro} , A , R , T , β and E_0 respectively denote the volume of adsorbate, the total volume of micropores, the differential free energy of adsorption, the perfect gas constant, the absolute temperature, the so-called similarity coefficient ($\beta = 0.33$ for nitrogen) and a characteristic

adsorption energy depending only on the adsorbent properties. The volume of mesopores, V_{meso} , is then estimated by subtracting V_{micro} from V_p . According to Stoeckli [27–29], the relation between the average width of the micropores, L_0 , and E_0 can be expressed according to the following empirical formula:

$$L_0 = 13.7/(E_0 - 9.7) \quad (4)$$

for $0.5 < L_0 < 2.5$ –3.0 nm, the standard deviation being $\sigma = 0.11$ nm [29].

The surface of the micropores, S_{micro} , can be calculated according to the following equation [27]:

$$S_{\text{micro}} = 2V_{\text{micro}}/L_0 \quad (5)$$

The α_S method is based on the comparison of the experimental physisorption isotherm of the studied porous sample to that of a non-porous material chosen as a reference. This method typically allows the determination of both the external surface area, S_{extl} , and the volume of the micropores, V_{micro} . In this work, α_S -plots were drawn using Vulcan 3 carbon as a reference material, which is a non-graphitized, non-porous carbon black [30] which has been used to establish early standard isotherms for studying porous carbons [31]. This reference material is appropriate to reveal the two swings of the high resolution α_S -plots [32] that are expected with the activated carbons under study that exhibit a pore size distribution going from the ultra micropores to mesopores [33, 34], contrary to some other reference materials such as black pearls [35], for instance. The question of matching the chemical properties of the reference carbon and of the carbon under study, in relation to the presence of heteroatoms, is still open. This is probably why authors use the same standard isotherm when constructing α_S -plots for porous carbons exhibiting quite different surface chemistries [36]. Progress on this question will probably be made when specific standard isotherms of non-porous carbons with well-characterised surface chemistry are published.

The fractal dimensions D_f , the notion of which is useful to interpret the adsorption of medium molecular size molecules from aqueous solutions [37], were determined by applying the equation:

$$\Phi = K \left\{ \ln \left(\frac{P}{P_0} \right) \right\}^{D_f - 3} \quad (6)$$

where Φ is the fractional filling at a relative pressure P/P_0 and K is a constant. This equation holds in the relative pressure range where the monolayer adsorption almost finishes on the pore walls ($P/P_0 < 0.05$) [38]. The form of this equation is the same as that of Frenkel–Halsey–Hill (FHH) which also applies to mesopore adsorption range [12]. Although the fractal dimension parameter determined for real world solids is not generally speaking interpretable

in the context of fractal self-similarity, this parameter complements the surface and pore size characterization and may provide clues to discuss surface roughness and accessibility to the adsorbate molecules from solution.

The PSDs were computed using the Micromeritics DFT software (DFT Plus(R) V2.02) considering the “carbon” model and assuming a slit-shaped geometry of the pores. This software is based on the Non-Localized Density Functional Theory (NLDFT) model.

5 Results

Figure 1 shows the PSDs obtained by mercury intrusion. It is seen that the PSD obtained within the pore width range $2.1\text{--}10^5\text{ nm}$ is very similar for F400 and IRHA. In contrast, the mesoporosity is more developed in PBL than in the two other ACs.

Figure 2 shows the nitrogen physisorption isotherms obtained for the ACs under study. It can be seen that F400 and IRHA show very similar nitrogen physisorption isotherms, F400 isotherm being slightly above that of IRHA. According to the IUPAC classification [25], these Type I isotherms indicate that F400 and IRHA have a highly developed microporous system. This is evidenced by the strong adsorption at very low relative pressures (i.e. $P/P_0 < 10^{-3}$). The hysteresis loop reveals the existence of mesopores; moreover, its Type H4 shape is, according to IUPAC, frequently associated with the presence of narrow slit-shaped pores. Furthermore, the two isotherms show a wide knee, spreading over the P/P_0 range $10^{-3}\text{--}0.2$, indicating that for both F400 and IRHA the PSD includes wider micropores. One can thus conclude that F400 and IRHA are essentially microporous ACs which have a large

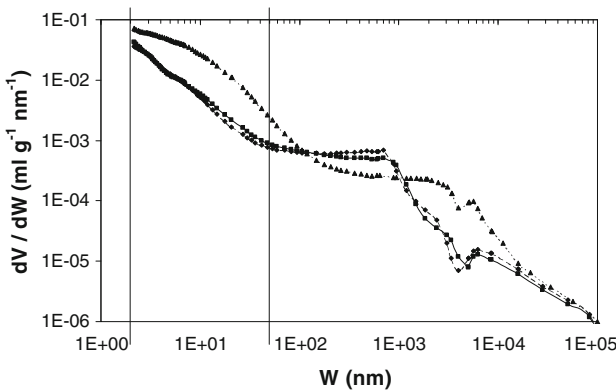


Fig. 1 Pore size distributions plotted as differential porous volume, dV/dW , versus apparent pore width, W , determined for F400 (■), IRHA (◆) and PBL (▲) using mercury porosimetry. The vertical lines show the boundaries (i) between micropores and mesopores and (ii) between mesopores and macropores, respectively

distribution of slit-shaped micropores which extends up to narrow mesopores.

Physisorption isotherm for PBL is much above those for F400 and IRHA and it shows a clearly different shape. This Type IV isotherm, with the presence of a wider hysteresis loop observed for relative pressures higher than 0.4, confirms the existence of a more developed mesoporosity in PBL than in F400 or IRHA. In addition, the strong adsorption observed at very low relative pressures (i.e. $P/P_0 < 0.001$) clearly indicates the additional presence of micropores in PBL. Finally, as observed in the lower relative pressure range, the micropore distribution is different for F400 and IRHA on the one hand, and PBL on the other hand (Fig. 2).

These qualitative results are confirmed by the DR analysis which results are shown in Table 3. The micro-porous volume is larger for PBL ($0.53\text{ cm}^3\text{ g}^{-1}$) than for F400 ($0.37\text{ cm}^3\text{ g}^{-1}$) or IRHA ($0.34\text{ cm}^3\text{ g}^{-1}$). The average pore width L_0 , which is equal to 2.1 nm, 1.0 nm and 1.1 nm for PBL, F400 and IRHA, respectively, follows the same trend. The values of micropore volumes provided by DR and α_S methods are in excellent agreement for F400 and IRHA. Although satisfactory, this agreement is not as good for PBL. This may stem from the fact that DR method relies on strong hypotheses while the second one is experimental but nevertheless dependent from the chosen non-porous reference carbon as stressed above.

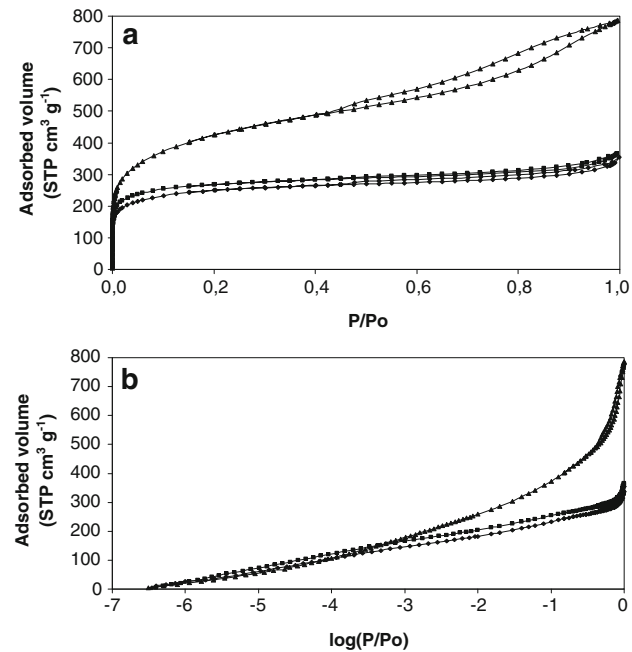


Fig. 2 Physisorption isotherms of N_2 at 77.4 K onto F400 (■), IRHA (◆) and PBL (▲). **a** in classical presentation; **b** with logarithmic abscissa showing the low pressure behaviour

Table 3 Values of E_0 , L_0 and of the different porous volumes ($\text{cm}^3 \text{g}^{-1}$) of F400, IRHA and PBL determined by various methods

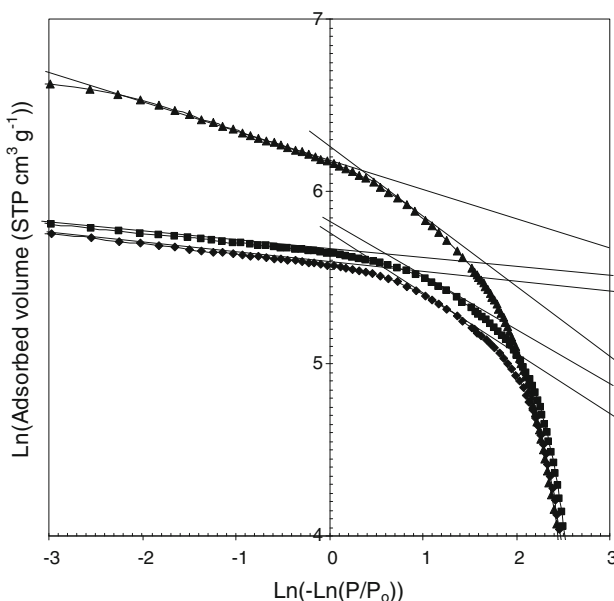
Activated carbon	V_p (at $P/P_0 = 0.995$)	V_{meso} (DR)	V_{meso} (α_S)	V_{micro} (DR)	V_{micro} (α_S)	V_{super} (α_S)	V_{ultra} (α_S)	E_0 (kJ mol^{-1}) (DR)	L_0 (nm) (DR)
F400	0.57	0.20	0.20	0.37	0.37	0.21	0.16	21.8	1.0
IRHA	0.55	0.21	0.21	0.34	0.34	0.21	0.13	21.3	1.1
PBL	1.22	0.69	0.80	0.53	0.42	0.30	0.12	16.5	2.1

Figure 3 shows the FHH plot for the three carbons under study. Fractal dimensions estimated from the slopes of the two linear parts seen in each curve are given in Table 4.

The values found for the fractal dimensions for carbon F400 are close to those reported by Garnier et al. [12]: 2.65 and 2.88 for the lower and higher P/P_0 ranges, respectively. The values found for IRHA are similar to those found for F400. For carbon PBL, the fractal dimensions are lower.

Contrary to the other methods considered in this study for textural analysis purposes, the α_S method proposed by Sing [23, 39] is only based on experimentation. Figure 4 shows the α_S -plots obtained for the three ACs examined. These plots exhibit two swings corresponding to primary and secondary pore fillings, respectively. Kaneko and coll. [40, 41] called these swings “filling swing” and “cooperative swing”, respectively.

From the slope and intercept of the linear part observed for $\alpha_S > 0.8$ (Fig. 4), one can calculate the external surface area, S_{ext1} , which corresponds to the total surface of macro- and meso-pores (pore width $> 2 \text{ nm}$) and the volume of micropores, V_{micro} , respectively. Moreover, according to Kaneko and coll. [34, 40–43], the slope of the straight line tangent to the α_S -plot (for α_S values in the range 0.4–0.6;

**Fig. 3** FHH plots for F400 (■), IRHA (◆) and PBL (▲)**Table 4** Fractal dimensions $D_f = 3 + h$ estimated from the slopes h of the straight lines drawn in Fig. 3

Activated carbon	Micropores	Mesopores
F400	2.67	2.94
IRHA	2.63	2.95
PBL	2.58	2.82

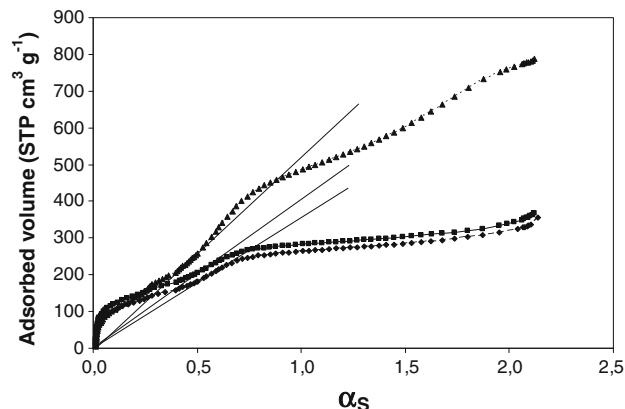
**Fig. 4** α_S plots obtained for F400 (■), IRHA (◆) and PBL (▲)

Fig. 4) and passing through the origin of the α_S plot is proportional to the total specific surface area of the solid. When determined this way, it will be termed S_T throughout this work. Therefore, these results allow the surface of the micropores, S_{micro} , and the volume of the mesopores, V_{meso} , to be estimated according to the following equations:

$$S_{\text{micro}} = S_T - S_{\text{ext1}} \quad (7)$$

$$V_{\text{meso}} = V_p - V_{\text{micro}} \quad (8)$$

Rouquerol et al. [44] proposed another interpretation of the α_S -plot. According to these authors, for $\alpha_S < 0.15$ (i.e. $P/P_0 < 2 \cdot 10^{-4}$), adsorbed nitrogen fills the ultramicropores; these micropores are the narrowest ones and they are defined as pores having an opening smaller than three times the diameter of the nitrogen molecule. Then, the linear part of the curve observed for α_S values in the range 0.15–0.45 corresponds to the adsorption of nitrogen on the walls of the supermicropores which are the widest micropores.

Table 5 Values of the different surface areas ($\text{m}^2 \text{ g}^{-1}$) of F400, IRHA and PBL determined by various methods

Activated carbon	S_{BET}	S_{T} [34]	S_{ext1} (α_S)	S_{ext2} (α_S)	S_{micro} (α_S)	S_{micro} (DR)	S_{super} (α_S)	S_{ultra} (α_S)
F400	1,012	1,025	118	537	907	717	419	488
IRHA	933	930	118	506	812	615	388	424
PBL	1,491	1,347	554	807	793	507	253	540

The non-linear part of the curve observed for α_S values in the average range 0.45–0.8 corresponds to the filling of the supermicropores. The second linear part of the curve observed for $\alpha_S > 0.8$ corresponds to the multilayer adsorption of nitrogen on a non-microporous surface. Thus, according to Rouquerol et al. [44], the slope and intercept of the linear part observed for α_S values in the range 0.15–0.45 give access to the surface area of pores wider than ultramicropores, termed S_{ext2} in the following, and to the volume of the ultramicropores, V_{ultra} , respectively. The surface area of the ultramicropores, S_{ultra} , the surface area of the supermicropores, S_{super} , and the volume of the supermicropores, V_{super} , can thus be estimated according to the following equations:

$$S_{\text{ultra}} = S_{\text{T}} - S_{\text{ext2}} \quad (9)$$

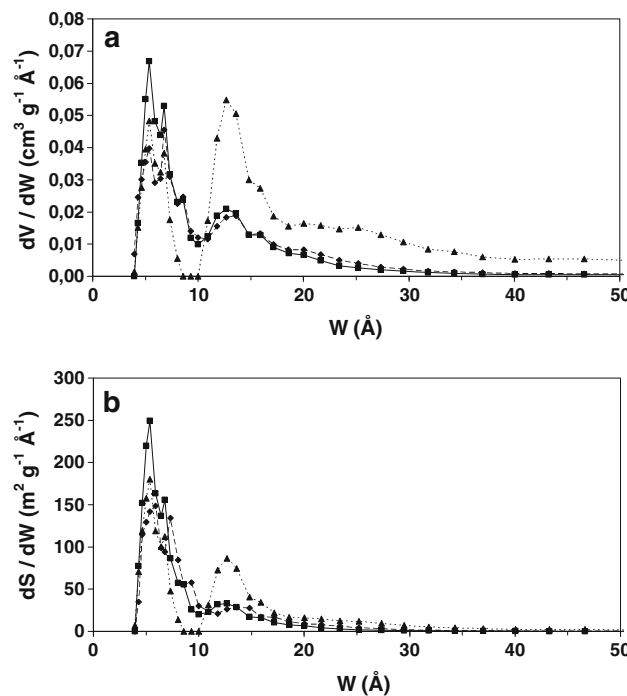
$$S_{\text{super}} = S_{\text{micro}} - S_{\text{ultra}} \quad (10)$$

$$V_{\text{super}} = V_{\text{micro}} - V_{\text{ultra}} \quad (11)$$

Tables 3 and 5 gather the textural characteristics of the three ACs we determined using the methods described above.

Figure 5 shows the PSD plots obtained using the DFT method and presented either as differential porous volume, dV/dW , or as differential surface area, dS/dW , versus pore width, W . These PSDs show two very close and rather sharp peaks and a wider peak respectively centred on the following W values: 0.5–0.6, 0.7 and 1.3 nm. In addition, for PBL the peak centred at 1.3 nm is much higher compared to the other ACs and the curve for $W > 2$ nm is clearly above those for F400 or IRHA. These patterns confirm that (i) the three ACs not only possess ultramicropores but also supermicropores, (ii) F400 and IRHA show very similar textural characteristics and (iii) PBL has a more developed mesoporosity. The values of the different pore volumes and surface areas deduced from the cumulative volume and cumulative surface area curves (curves not shown) are presented in Table 6.

Table 7 shows the contributions of V_{micro} and S_{micro} to the porous structure of F400, IRHA and PBL, respectively, as found by α_S and DFT methods (Tables 3, 5, 6). For this last method, 2 nm has been taken as the micropore maximum width. It is seen that there is a satisfactory agreement between the results provided by the two methods, although

**Fig. 5** Pore size distributions plotted as **a** differential porous volume, dV/dW ; and **b** differential surface area, dS/dW , versus pore width, W , determined for F400 (■), IRHA (◆) and PBL (▲) using DFT method**Table 6** Specific surface areas and pore volumes (in italic) obtained with the DFT method for F400, IRHA and PBL

		0–0.7 nm	0–1 nm	0–2 nm	0–50 nm	S_{Total}
						V_{Total}
F400	$(\text{m}^2 \text{ g}^{-1})$	490	616	793	829	830
	$(\text{cm}^3 \text{ g}^{-1})$	0.14	0.19	0.32	0.41	0.42
IRHA	$(\text{m}^2 \text{ g}^{-1})$	400	533	704	759	760
	$(\text{cm}^3 \text{ g}^{-1})$	0.11	0.17	0.29	0.43	0.47
PBL	$(\text{m}^2 \text{ g}^{-1})$	370	389	788	1,030	1,030
	$(\text{cm}^3 \text{ g}^{-1})$	0.10	0.11	0.40	1.04	1.05

Table 7 Contribution (%) of V_{micro} and S_{micro} to the porous structure of F400, IRHA and PBL

	α_S	DFT	α_S	DFT
	V_{micro}/V_p	$V_{\text{micro}}/V_{\text{Total}}$	$S_{\text{micro}}/S_{\text{T}}$	$S_{\text{micro}}/S_{\text{Total}}$
F400	65	75	87	96
IRHA	62	61	88	93
PBL	34	38	59	77

the ratios obtained from the DFT results are most of the time higher than those provided by the α_S method. The reason might be that the DFT method provides underestimated values of mesopore surfaces and volumes. As the α_S

method is an experimental one based on very few assumptions, one may think that it is rather the DFT method that overestimates the proportion of the micropores.

Table 7 also shows that the contribution of the external surface area (total surface of pores having a width >2 nm; $S_{\text{ext}} = S_T - S_{\text{micro}}$) is much more important for PBL than for F400 or IRHA. This result is consistent with both the PSD obtained from the mercury intrusion experiments and the conclusions drawn from the discussion of the shape of the nitrogen physisorption isotherms; this result confirms the more developed mesoporosity of PBL.

6 Discussion

6.1 Specific surface areas

The values of S_{BET} and V_p measured in this work, $1,012 \text{ m}^2 \text{ g}^{-1}$ (P/P_0 range $0.01\text{--}0.1$) and $0.57 \text{ cm}^3 \text{ g}^{-1}$ ($P/P_0 = 0.995$), respectively, are very close to the mean values calculated from Table 2, i.e. $1,005 \text{ m}^2 \text{ g}^{-1}$ and $0.58 \text{ cm}^3 \text{ g}^{-1}$. The mean microporous volume from literature data is $0.4 \text{ cm}^3 \text{ g}^{-1}$. It is close to that we found, i.e., $0.37 \text{ cm}^3 \text{ g}^{-1}$, by two independent methods, DR and α_S . Therefore, these values can be considered to be typical of F400. In addition, it is confirmed that the fractal dimension determined with points of the nitrogen isotherm close to monolayer completion is about 2.65.

It is of interest to consider how S_{BET} depends on the P/P_0 range used for its determination. This point has been addressed, for instance, by Kaneko and Ishii [41] in a work on activated mesophase carbon microbeads (AMCM) variously activated. These authors showed that the S_{BET} value may strongly depend on the P/P_0 range used for its determination. Thus, for samples having high surface areas ($>1,800 \text{ m}^2 \text{ g}^{-1}$), S_{BET} values showed a dramatic increase (up to 40%) when the relative pressure range shifted from $2.10^{-3}\text{--}10^{-2}$ to $0.1\text{--}0.3$. In contrast, S_{BET} values were nearly constant for samples having lower surface areas (about $500 \text{ m}^2 \text{ g}^{-1}$). In addition, Kaneko and Ishii [41] observed that S_{BET} value determined near $P/P_0 = 0.01$ is almost the same as the S_T value.

Figure 6 shows how the values we found for S_{BET} depend on the range of P/P_0 chosen for their determination. Our results are quite consistent with those of Kaneko and Ishii [41]. Indeed, the behaviour observed for PBL resembles that of AMCM having a surface area S_T approximately equal to $1,800 \text{ m}^2 \text{ g}^{-1}$ while the behaviours observed for both F400 and IRHA are similar to that of AMCM having lower S_T values (about $500 \text{ m}^2 \text{ g}^{-1}$). The differences in the behaviour of all these samples are likely due to various activation degrees associated with different

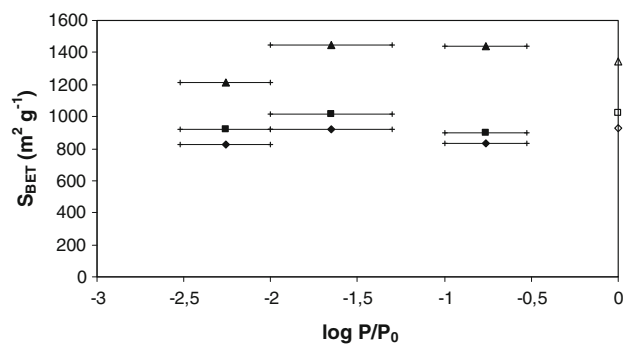


Fig. 6 Dependence of S_{BET} value upon the P/P_0 range chosen for its determination for F400 (■), IRHA (◆) and PBL (▲). Empty symbols: specific surface areas S_T calculated from the α_S plot

distributions of micropore widths. Indeed, in Kaneko and Ishii's paper [41], a large increase of S_{BET} with the shift of P/P_0 range toward higher values is observed with samples showing a highly developed cooperative swing in the α_S plot. In this case, S_{BET} largely overestimates the specific surface area. This is not the case for F400 or for IRHA (Fig. 4).

It is worth noting that the behaviour observed for our samples (coal physically activated or wood chemically activated) can be compared to those obtained for AMCM although these samples are supposed to exhibit different structural orders (size, stacking and mutual position of the graphene layers) and heteroatom contents. Hence, the consistency of the results reported by Kaneko and Ishii [41] and ours as shown in Fig. 6 does not seem to be fortuitous and therefore it would be interesting to further investigate this point using other AC samples.

Apart from that, Stoeckli and Centeno [5] proposed a criterion to assess the accuracy of the S_{BET} value after they compared the values of S_{BET} and the specific surface areas they found by some other methods (i.e. immersion calorimetry and CO_2 adsorption at 25°C) for numerous ACs. These authors proposed that the value of S_{BET} represents the correct specific surface area if the DR width, L_0 , lays in the range $0.8\text{--}1.1 \text{ nm}$. S_{BET} provides an overestimated value of the specific surface area if L_0 is above this range and an underestimated value in the opposite case. Back to our results, and taking into account the standard deviation $\sigma = 0.11 \text{ nm}$, the values of L_0 found for F400 and IRHA are in the upper limit of this range, which means that Stoeckli and Centeno criterion can be considered as verified for these two ACs (Table 3). In contrast, this criterion is not satisfied for carbon PBL for which $L_0 = 2.1$. Thus, the S_{BET} value found for PBL would overpass the specific surface area, especially if it is determined in the range $P/P_0 = 0.1\text{--}0.3$, the domain which is frequently chosen for its assessment.

Previously to the work of Stoeckli, and Centeno, Setoyama et al. [34] proposed a classification of the α_S plots into four typical types according to their shape. This classification, based on theoretical simulations, is accompanied by a discussion about the correctness of the use of S_T , determined from the α_S plot, for specific surface area estimation. Applying these considerations to the α_S plot of F400 (Fig. 4), it can be deduced that F400 exhibits an intermediate shape between Type MS (Molecular Sieve) and Type R (Representative of ACs). Type MS is typical of a carbon having narrow micropores (pore width <0.7 nm) and a sharp PSD. Type R corresponds to a PSD with a maximum at 0.9 nm accompanied by a much lower secondary peak near 2 nm. Accepting, after Kaneko's work, that it is possible to determine the specific surface area from the slope of the line connecting the origin and the edge of the step in Type MS α_S plots, and that the line connecting the origin to the linear region in the α_S range 0.5–0.7 provides an only slightly overestimated specific surface area in Type R α_S plots, it can be concluded that the value of S_T assessed for F400 is close to the accurate specific surface area of this AC.

As the S_{BET} value of F400 does not dramatically increase with the shift of the P/P_0 range toward higher values on the one hand, and as S_{BET} is very close to S_T on the other hand (Table 5), it can be concluded that the value of $1,012\text{ m}^2\text{ g}^{-1}$ results from a correct assessment of the specific surface area of F400. The same arguments hold for IRHA and consequently it can be concluded that the value of $930\text{ m}^2\text{ g}^{-1}$ is a correct assessment of its specific surface area.

Concerning PBL, its α_S plot (see Fig. 4) exhibits an intermediate shape between Type R and Type B (Bimodal). For this last type, according to Setoyama et al. [34], the slope of the line passing through the origin and the transition point between the filling and the cooperative swings leads to a correct estimation of the specific surface area. Consequently, after Setoyama et al. [34], it could be concluded that the value $S_T = 1,350\text{ m}^2\text{ g}^{-1}$ is a correct assessment of the specific surface area of PBL. It is indeed smaller than S_{BET} ($1,491\text{ m}^2\text{ g}^{-1}$) as predicted by Stoeckli's criterion mentioned above.

6.2 Pore size distribution

Table 6 shows the pore volumes and surface areas obtained for given ranges of pore widths and determined from the PSD provided by the DFT method. The values found for F400 in the present work are in a good agreement with those published by Dastgheib et al. for both volumes [45] and areas [11].

From Table 6, one can see that the total specific surface area estimated by DFT, S_{Total} , is smaller than S_{BET}

(Table 5) for the three ACs under study. The discrepancy between S_{Total} and S_{BET} is commonly observed in the literature. For instance, Shi [46] studying 34 AC samples observed that S_{BET} values were systematically higher than S_{Total} values determined with the Micromeritics DFT software. The same conclusion can be drawn from the results obtained by Dastgheib et al. [11] for 25 original and modified ACs. Therefore, the total specific surface areas found for ACs using the NLDFT model (as in the Micromeritics software) are likely to be underestimated.

Another typical feature of the PSD obtained by DFT is the presence of a marked gap for a pore width of about 1 nm. This feature has been observed in numerous instances [47, 48]. It has been shown to be an artefact of the NLDFT method in which smooth surfaces of pore walls are postulated [49] while real surfaces of AC pore walls exhibit some roughness.

7 Conclusions

The textural characteristics of Filtrasorb 400, an activated carbon widely used in water treatment and often considered as a reference adsorbent in fundamental studies about pollutant removal from aqueous solutions, have been reviewed. From literature data, the mean values of S_{BET} , V_p and V_{micro} are $1,005\text{ m}^2\text{ g}^{-1}$, $0.58\text{ cm}^3\text{ g}^{-1}$ and $0.4\text{ cm}^3\text{ g}^{-1}$, respectively, with corresponding standard deviations of about 10% for S_{BET} and V_p , and 15% for V_{micro} . They are close to the values we determined in the present study, i.e., $1,012\text{ m}^2\text{ g}^{-1}$, $0.57\text{ cm}^3\text{ g}^{-1}$ and $0.37\text{ cm}^3\text{ g}^{-1}$, respectively.

From our experimental results, it can be seen that activated carbon IRHA exhibits textural characteristics close to those of F400 as both activated carbons show a wide distribution of micropores which spreads from ultramicropores up to narrow mesopores. Nevertheless, the specific surface area and pore volume of IRHA are slightly smaller than those of F400. PBL activated carbon is quite different from the two others as its microporosity and mesoporosity are more developed.

The interpretation of α_S -plots proposed by Kaneko and collaborators, as well as a criterion given by Stoeckli and Centeno allowed us to better understand the meaning of S_{BET} , the specific surface area determined by the popular BET method. From our results, it is possible to conclude that the accurate specific surface area of F400, as estimated from nitrogen physisorption, may be assessed to $1,010\text{ m}^2\text{ g}^{-1}$ for samples outgassed at 120°C under high vacuum.

The same critical examination of the textural results obtained for IRHA and PBL led us to the conclusion that $S_{BET} = 920\text{ m}^2\text{ g}^{-1}$ is a correct assessment of the specific

surface area for IRHA while $S_{\text{BET}} = 1,491 \text{ m}^2 \text{ g}^{-1}$ is an overestimated value of the specific surface area of PBL which is likely to be $1,350 \text{ m}^2 \text{ g}^{-1}$.

The complete set of textural results described in the present work will be used to interpret the results we obtained about the adsorption of medium molecular weight pollutants from aqueous solution mainly in terms of the accessibility of the microporosity of the activated carbons to the considered adsorbates.

Acknowledgments The authors wish to thank Chemviron Carbon (European Operations of Calgon Carbon Corporation, USA) and Pica (France) who kindly provided them with the activated carbon samples. Authors wish to thank Noëlle Cristin (IRCELYON) and Camille Schlitter (Institut Français du Pétrole) who performed the nitrogen physisorption and the mercury porosimetry experiments, respectively. The corresponding author also gratefully acknowledges kind encouragement from James Hickman, Director of the NanoScience Technology Center (NSTC, University of Central Florida, USA), during her stay at NSTC.

References

1. F.C. Wu, R.L. Tseng, C.C. Hu, *Micropor. Mesopor. Mater.* **80**, 95 (2005)
2. S.I. Kim, T. Yamamoto, A. Endo, T. Ohmori, M. Nakaiwa, *Micropor. Mesopor. Mater.* **96**, 191 (2006)
3. D. Graham, *J. Phys. Chem.-US* **59**, 896 (1955)
4. L.M. Pastrana-Martinez, M.V. Lopez-Ramon, C. Moreno-Castilla, *J. Colloid Interf. Sci.* **331**, 2 (2009)
5. F. Stoeckli, T.A. Centeno, *Carbon* **43**, 1184 (2005)
6. N. Passé-Coutrin, S. Altenor, S. Gaspard, *J. Colloid Interf. Sci.* **332**, 515 (2009)
7. D.C.W. Tsang, J. Hu, M.Y. Liu, W.H. Zhang, K.C.K. Lai, I.M.C. Lo, *Water Air Soil Pollut.* **184**, 141 (2007)
8. Y.S. Al-Degs, M.I. El-Barghouthi, M.A. Khraisheh, M.N. Ahmad, S.J. Allen, *Sep. Sci. Technol.* **39**, 97 (2004)
9. P.M. Alvarez, J.F. Garcia-Araya, F.J. Beltran, F.J. Masa, F. Medina, *J. Colloid Interf. Sci.* **283**, 503 (2005)
10. P. Canizares, M. Carmona, O. Baraza, A. Delgado, M.A. Rodríguez, *J. Hazard. Mater.* **131**, 243 (2006)
11. S.A. Dastgheib, T. Karanfil, W. Cheng, *Carbon* **42**, 547 (2004)
12. C. Garnier, T. Gorner, A. Razafitianamaharavo, F. Villieras, *Langmuir* **21**, 2838 (2005)
13. Q. Lu, G.A. Sorial, *Carbon* **42**, 3133 (2004)
14. G. Newcombe, M. Drikas, *Carbon* **35**, 1239 (1997)
15. J. Rivera-Utrilla, M. Sanchez-Polo, *Carbon* **40**, 2685 (2002)
16. G. Skodras, I. Diamantopoulou, P. Natas, A. Palladas, G.P. Sakellaropoulos, *Energ. Fuel* **19**, 2317 (2005)
17. Z. Yue, J. Economy, G. Bordson, *J. Mater. Chem.* **16**, 1456 (2006)
18. G. Newcombe, Carbon round robin international inter-laboratory try for the determination of activated carbon pore volume distributions. Visited on July 29, 2009. Available from: http://www.waterquality.crc.org.au/carbon_rr/round_robin_index.htm
19. P.C. Hiemenz, *Principles of Colloid and Surface Chemistry*, vol. 2 (Marcel Dekker, New York, 1986)
20. J.I. Paredes, A. Martinez-Alonso, P.X. Hou, T. Kyotani, J.M.D. Tascon, *Carbon* **44**, 2469 (2006)
21. S. Brunauer, P.H. Emmett, E. Teller, *J. Am. Chem. Soc.* **60**, 309 (1938)
22. M.M. Dubinin, *Prog. Surf. Membrane Sci.* **9**, 1 (1975)
23. K.S.W. Sing, *Chem. Ind.* 1520 (1968)
24. K.E. Gubbins, *NATO ASI Series, Series C: Math. Phys. Sci.* **491**, 65 (1997)
25. K.S.W. Sing, D.H. Everett, R.A.W. Haul, L. Moscou, R.A. Pierrotti, J. Rouquerol et al., *Pure Appl. Chem.* **57**, 603 (1985)
26. M.M. Dubinin, L.V. Radushkevich, *Doklady Akad. Nauk SSSR* **55**, 327 (1947)
27. F. Stoeckli, in *Porosity in Carbons-Characterization and Applications*, ed. by J. Patrick (Arnold, London, 1995), p. 67
28. F. Stoeckli, E. Daguerre, A. Guillot, *Carbon* **37**, 2075 (1999)
29. F. Stoeckli, M.V. Lopez-Ramon, D. Hugi-Cleary, A. Guillot, *Carbon* **39**, 1115 (2001)
30. P.L. Walker Jr., W.V. Kotlensky, *Can. J. Chem.* **40**, 184 (1962)
31. P.J.M. Carrott, R.A. Roberts, K.S.W. Sing, *Carbon* **25**, 59 (1987)
32. X. Py, A. Guillot, B. Cagnon, *Carbon* **41**, 1533 (2003)
33. K. Kaneko, *J. Membrane Sci.* **96**, 59 (1994)
34. N. Setoyama, T. Suzuki, K. Kaneko, *Carbon* **36**, 1459 (1998)
35. M. Kruk, M. Jaroniec, J. Choma, *Carbon* **36**, 1447 (1998)
36. A. Derylo-Marczewska, A. Świątkowski, S. Biniak, M. Walczyk, *Colloid Surface A* **327**, 1 (2008)
37. N.R. Khalili, M.Z. Pan, G. Sandi, *Carbon* **38**, 573 (2000)
38. M. Sato, T. Sukegawa, T. Suzuki, K. Kaneko, *J. Phys. Chem. B* **101**, 1845 (1997)
39. K.S.W. Sing, in *Surface Area Determination*, ed. by D.H. Everett, R.H. Ottewill (Butterworths, London, 1970), p. 25
40. K. Kaneko, C. Ishii, *Colloid. Surface* **67**, 203 (1992)
41. K. Kaneko, C. Ishii, M. Ruike, H. Kuwabara, *Carbon* **30**, 1075 (1992)
42. K. Murata, K. Kaneko, F. Kokai, K. Takahashi, M. Yudasaka, S. Iijima, *Chem. Phys. Lett.* **331**, 14 (2000)
43. M. El-Merraoui, M. Aoshima, K. Kaneko, *Langmuir* **16**, 4300 (2000)
44. F. Rouquerol, L. Luciani, P. Llewellyn, R. Denoyel, J. Rouquerol, in *Génie des Procédés*, vol. P 1050 (Techniques de l'Ingénieur, Paris, 2003), pp. 1–24
45. S.A. Dastgheib, T. Karanfil, *J. Colloid Interf. Sci.* **274**, 1 (2004)
46. H. Shi, *Electrochim. Acta* **41**, 1633 (1996)
47. P. Chingombe, B. Saha, R.J. Wakeman, *Carbon* **43**, 3132 (2005)
48. P. Chingombe, B. Saha, R.J. Wakeman, *J. Colloid Interf. Sci.* **302**, 408 (2006)
49. P.I. Ravikovich, M. Thommes, A.V. Neimark, in *Carbon 2007 Conference*, Seattle, WA, ed. by The American Carbon Society, CD-Rom Proceedings (Omnipress, Madison, WI, 2007), p. B141(K)